TOXICOLOGICAL SCIENCES **126(2)**, 457–468 (2012)
doi:10.1093/toxsci/kfs003
Advance Access publication January 12, 2012

Effects of Silver Nanoparticles on Primary Mixed Neural Cell Cultures: Uptake, Oxidative Stress and Acute Calcium Responses

Andrea Haase,*[,1] Stephanie Rott,† Alexandre Mantion,‡ Philipp Graf,§ Johanna Plendl,¶ Andreas F. Thünemann,‡ Wolfgang P. Meier,§ Andreas Taubert,||,|||, Andreas Luch,* and Georg Reiser†

*Department of Product Safety, German Federal Institute for Risk Assessment (BfR), 10589 Berlin, Germany; †Institute of Neurobiochemistry, University of Magdeburg, 39120 Magdeburg, Germany; ‡Division 6.5, Polymers in Life Science and Nanotechnology, BAM Federal Institute for Materials Research and Testing, 12205 Berlin, Germany; §Department of Chemistry, University of Basel, 4056 Basel, Switzerland; ¶Department of Veterinary Medicine, Institute of Veterinary Anatomy, Free University Berlin, 14195 Berlin, Germany; ||Institute of Chemistry, University of Potsdam, 14476 Potsdam-Golm, Germany; and |||Max-Planck-Institute of Colloids and Interfaces, 14476 Potsdam-Golm, Germany

[1]To whom correspondence should be addressed. Fax: +49-30-18412-4928. E-mail: andrea.haase@bfr.bund.de.

Received August 16, 2011; accepted January 2, 2012

In the body, nanoparticles can be systemically distributed and then may affect secondary target organs, such as the central nervous system (CNS). Putative adverse effects on the CNS are rarely investigated to date. Here, we used a mixed primary cell model consisting mainly of neurons and astrocytes and a minor proportion of oligodendrocytes to analyze the effects of well-characterized 20 and 40 nm silver nanoparticles (SNP). Similar gold nanoparticles served as control and proved inert for all endpoints tested. SNP induced a strong size-dependent cytotoxicity. Additionally, in the low concentration range (up to 10 μg/ml of SNP), the further differentiated cultures were more sensitive to SNP treatment. For detailed studies, we used low/medium dose concentrations (up to 20 μg/ml) and found strong oxidative stress responses. Reactive oxygen species (ROS) were detected along with the formation of protein carbonyls and the induction of heme oxygenase-1. We observed an acute calcium response, which clearly preceded oxidative stress responses. ROS formation was reduced by antioxidants, whereas the calcium response could not be alleviated by antioxidants. Finally, we looked into the responses of neurons and astrocytes separately. Astrocytes were much more vulnerable to SNP treatment compared with neurons. Consistently, SNP were mainly taken up by astrocytes and not by neurons. Immunofluorescence studies of mixed cell cultures indicated stronger effects on astrocyte morphology. Altogether, we can demonstrate strong effects of SNP associated with calcium dysregulation and ROS formation in primary neural cells, which were detectable already at moderate dosages.

Key Words: **silver nanoparticles; neurons; oxidative stress; protein carbonyls; calcium.**

Because of their antimicrobial, optical, and catalytic properties, silver nanoparticles (SNP) have gained particular interest for many commercial applications. According to the Woodrow Wilson inventory, approximately 30% of all nanoparticle-enabled products contain nanosilver. Thus, SNP are highly commercialized and are now being used in many daily life products mainly because of their antimicrobial properties (Chen and Schluesener, 2008). SNP are incorporated in textiles, used in cosmetics, or as coatings in various household goods. In the medical fields, SNP are applied in wound disinfection and in antibacterial coatings of medical devices or prostheses. In clear contrast to their widespread use, putative health effects have only just begun of being adequately addressed.

Serious concerns arise because nanoparticles may not only cause adverse effects in primary organs directly exposed but also in secondary organs, such as the cardiovascular or central nervous system (CNS) (Kreyling *et al*., 2006), upon systemic distribution. Nanoparticles can reach the CNS via different routes (reviewed in Oberdörster *et al*., 2009). For instance, as breathable fraction, nanoparticles can reach the brain through the upper respiratory tract via the olfactory bulb as it has been demonstrated for manganese oxide nanoparticles in rats (Elder *et al*., 2006). This has also been documented for SNP (Ji *et al*., 2007). Through other exposure routes, e.g., subcutaneous injection, SNP may reach the brain as well (Tang *et al*., 2009). Discussions are still ongoing of whether or not nanoparticles may pass the intact blood-brain barrier (BBB) by an as yet unknown mechanism. It has been shown that SNP can translocate through and accumulate in an *in vitro* BBB model composed of rat brain microvessel vascular endothelial cells (Tang *et al*., 2010). In another study, SNP induced inflammation and affected the integrity of a BBB model composed of primary rat brain microvessel endothelial cells (Trickler *et al*., 2010). There is also evidence that certain nanoparticles made of copper or silver can disrupt the BBB *in vivo* (Sharma and Sharma, 2007). However, the fraction of nanoparticles that may reach the brain via systemic circulation is expected to be rather low under healthy conditions, whereas the fraction translocated into the brain via sensory nerve

© The Author 2012. Published by Oxford University Press on behalf of the Society of Toxicology. For permissions, please email: journals.permissions@oxfordjournals.org.
This is an Open Access article distributed under the terms of the Creative Commons Attribution Non-Commercial License (http://creativecommons.org/licenses/by-nc/3.0), which permits unrestricted non-commercial use, distribution, and reproduction in any medium, provided the original work is properly cited.

Downloaded from http://toxsci.oxfordjournals.org/ at Bundesinstitut fuer Gesundheitlich on July 24, 2014

endings in the olfactory bulb during inhalation may be quite significant in comparison (Oberdörster *et al.*, 2004). Upon systemic distribution, depending on the study design, the particle type and the route of administration between 0.1 and 3% of the retained fraction can be detected in secondary target organs, such as liver, spleen, kidney, or brain (Chen *et al.*, 2006; Kreyling *et al.*, 2009). Importantly, this fraction may increase, for instance, under inflammatory conditions. Only rarely has the translocation of nanoparticles into the brain been studied using models that express a compromised BBB. Under such conditions, an increase in brain translocation of 160–290% was detectable for certain nanoparticles, such as iron oxide (Rousseau *et al.*, 1997). If rats were pretreated with proinflammatory lipopolysaccharides prior to the intratracheal instillation of nanoparticles, up to 10% (compared with 3% in healthy animals without inflammation) were translocated to the liver (Chen *et al.*, 2006). Importantly, also, the particle properties have an influence on particle translocation. In an *in vivo* study applying 12 nm gold nanoparticles (GNP), the brain delivery was found to increase by fourfold when using a peptide coating instead of the conventional citrate coating (Guerrero *et al.*, 2010). Finally, it is unclear whether nanoparticles will accumulate in the brain under repeated or chronic exposures. For bulk materials, it has already been known for a long time that certain elements such as silver have a prolonged half-life in the CNS compared with other organs (Rungby and Danscher, 1983).

Nanoparticles possess an increased surface to volume ratio and thus display a much higher reactivity compared with the corresponding bulk material. They strongly differ in their physicochemical properties and tend to behave differently in biological systems. As a general paradigm deduced from several *in vitro* and *in vivo* studies, responses via oxidative stress and/or inflammation seem the most likely outcome (Arora *et al.*, 2008; Carlson *et al.*, 2008; Chen *et al.*, 2007). A few *in vivo* studies analyzed the effects of nanoparticles in the brain. The observed effects can be categorized as inflammation and oxidative stress. For instance, under *in vivo* conditions, manganese oxide (inhalation) induced inflammation in rat brain (Elder *et al.*, 2006), silver (ip) caused oxidative stress and upregulation of oxidative stress–related genes in the cortex and hippocampus of mice (Rahman *et al.*, 2009), or buckminsterfullerene C60 particles suspended in water (nC60) caused lipid peroxidation and total glutathione decrease in fish brain (Oberdörster *et al.*, 2004). It should be emphasized that the brain is especially vulnerable to oxidative stress. Oxidative stress is involved in the pathogenesis of many neurodegenerative diseases, such as Alzheimer's disease, Parkinson's disease, or Huntington's disease (Mates *et al.*, 1999). Therefore, the effects of nanoparticles in neural cells should be carefully analyzed. Still, only few *in vitro* studies have been published, which typically use neural-like cell lines. Mostly, PC-12 cells (rat cell line with a neuronal-like phenotype) are used or, less frequently, other cell lines such as BV2 (mouse microglia) or N27 (rat dopaminergic neurons). Only some studies used primary neural cells (e.g., Gramowski *et al.*, 2010; Liu *et al.*, 2009, 2011; Zhaowei *et al.*, 2009).

Changes in gene expression and interference with signal transduction pathways are documented for neuronal cell lines, such as PC-12, after treatment with silver or copper nanoparticles (Hussain *et al.*, 2006; Wang *et al.*, 2009). One study has analyzed responses of primary neural networks, originating from frontal cortices of mice, upon treatment with nanoparticles (titanium dioxide, carbon black, and hematite) and proved its interference with electric activities (Gramowski *et al.*, 2010). Two studies used primary CA1 neurons from mice and demonstrated interference of SNP with action potentials via voltage-gated sodium (Zhaowei *et al.*, 2009) or potassium channels (Liu *et al.*, 2009, 2011).

In the present study, we analyzed for the first time the effects of SNP on mixed primary neural cells. We focused on the uptake of the particles and on oxidative stress and calcium responses. Oxidative stress in neural cells is of particular interest because it is regarded as a key modulator in several neurodegenerative diseases. Our experiments reveal different measurable endpoints of SNP-mediated oxidative stress development within different time frames. For the first time, we demonstrate an acute calcium response in cells upon SNP treatment, which apparently precedes the onset of oxidative stress. Our results suggest that nanoparticles would directly interfere with calcium-based signaling processes in neural tissue once reaching the brain.

MATERIALS AND METHODS

Synthesis of nanoparticles. Chemicals were obtained in pro analysi, analytical grade quality from Bachem (Bubendorf, Switzerland) or Fluka (Buchs, Switzerland) and used without further purification. All amino acids were L-isomers. The synthesis and the characterization of the nanoparticles have been recently described in detail (Graf *et al.*, 2009). Briefly, after synthesis, they were purified by repeated centrifugation-redispersion prior to freeze-drying. In the experiments, we used two differently sized peptide-coated SNP, i.e., 20 nm (Ag_{20}Pep) and 40 nm (Ag_{40}Pep). The results were compared with corresponding 20 nm peptide-coated GNP (Au_{20}Pep). Au_{20}Pep particles were prepared via ligand exchange of citrate-coated GNP.

Characterization of nanoparticles. Particles were characterized by several methods after freeze-drying. Transmission electron microscopy (TEM) images were taken at an FEI Morgani 268D operated at 80 kV. Samples were deposited on carbon-coated copper grids and directly imaged after drying in air. Some samples were diluted prior to imaging to allow for better imaging conditions. Small-angle X-ray scattering (SAXS) measurements were performed with a SAXSess camera (Anton Paar, Austria) attached to a laboratory X-ray generator (PW3830, PANanalytical) operated with a fine focus glass X-ray tube at 40 kV and 50 mA (CuKα, $\lambda = 0.1542$ nm). Samples were filled in a reusable vacuum tight 1-mm quartz capillary to attain the same scattering volume and background contribution. Data were analyzed as published elsewhere (Graf *et al.*, 2009). Size distributions were analyzed via dynamic light scattering (DLS) performed on particle dispersions in distilled water or in complete cell culture medium at room temperature in a Zetasizer ZS (Malvern Instruments, UK). Samples were not filtered prior to measurements. The laser wavelength was 633 nm, and data were recorded in a backscattering mode at $2\theta = 173°$. Optical properties of bulk metallic silver and gold were used for data analysis (Johnson and Christy, 1972). The metal content of one nanoparticle was

Downloaded from http://toxsci.oxfordjournals.org/ at Bundesinstitut fuer Gesundheitlich on July 24, 2014

determined at about 95% of the weight. Possible contamination by endotoxins was assessed with LAL endotoxin kit (Lonza, Germany). The particles were found to be free of endotoxins (containing less than 0.01 endotoxin units/ml stock suspension).

Suspension of nanoparticles. Nanoparticle aliquots were stored and freeze-dried at −80°C. Suspensions of particles were freshly prepared before each experiment. Aliquots of SNP were first resuspended in acidified water with ultrasonication and then diluted in cell culture medium.

Cell culture. All experimental conditions for the rats were according to the Guidelines for Proper Control of Animal Experiments approved by the local ethics committee and were planned to minimize the number of animals used. Primary cultures of neurons from cortex were obtained from brains of 1- to 3-day-old Wistar rats according to a protocol published elsewhere (Wang *et al.*, 2007). Briefly, the cerebral cortices were isolated, cut into small pieces, and incubated with papain (20 U/ml) in ice-cold Puck's-D1 solution containing the following ingredients: 137.0mM NaCl, 5.4mM KCl, 0.2mM KH_2PO_4, 0.17mM Na_2HPO_4, 5.0mM glucose, 58.4mM sucrose, pH 7.4, at 37°C for 7 min. The digested cortical pellets were gently washed once and suspended in ice-cold Puck's-D1 solution. Subsequently, the cell suspension was collected after filtering through a 136-µm mesh. After centrifugation at 300 × g for 5 min, cells were resuspended in 6 ml neurobasal A medium (containing B27 supplement, 5 ng/ml basic fibroblast growth factor, 0.5mM L-alanyl-L-glutamine, 100 U/ml penicillin, and 100 µg/ml streptomycin), plated on poly-L-lysine-coated dishes, and cultured in a humidified incubator with 5% CO_2 at 37°C for 2 h. Afterward, the medium was aspirated to remove additional debris and replaced with fresh complete neurobasal A medium. Half of the medium was changed every 3–4 days. For some of the cultures at day 1 or 2 after plating, cytosine arabinoside (AraC, 10^{-5}M) was added to suppress the growth of glial cells. For pretreatment with *N*-acetylcysteine (NAC), cells were incubated with a final concentration of 10mM for 1 h before the nanoparticles were added.

The astrocyte cultures were obtained from total rat brains, as described in Wang *et al.* (2007). The cells were seeded in Dulbecco's Modified Eagle's Medium complemented with 10% fetal bovine serum (obtained from Biochrome, Berlin, Germany). The medium was changed every 3 days. After 10 days in culture, the cells were detached and seeded in the cell culture vessels for the experiments. These cultures were characterized to contain more than 90% astrocytes.

WST-1 cell viability assay/lactate dehydrogenase assay. All assays were carefully established to avoid nanoparticle-induced interferences. Cells were seeded in 96-well format and then allowed to grow and differentiate for 1, 2, or 3 weeks before treatment. Nanoparticles (Ag_{20}Pep, Ag_{40}Pep, and Au_{20}Pep) were tested in concentrations of 5–100 µg/ml for 24 h of incubation. For the lactate dehydrogenase (LDH) assay, the supernatant was removed, centrifuged, and analyzed with LDH assay from Roche Diagnostics (Mannheim, Germany). As a positive control, cells were completely lysed with Triton X-100 according to the manufacturer's instructions. For the WST-1 assay, WST-1 reagent was added and after 3 h of incubation, supernatants were transferred into vials, and centrifuged with maximum speed at room temperature in a tabletop centrifuge (Eppendorf, Hamburg, Germany) to remove interfering particles (16,800 × g). After centrifugation, spectrophotometric readout was performed. For the WST-1 assay, two positive chemical controls were included (1mM hydrogen peroxide and 200µM glutamate). WST-1 reagent was purchased from Roche Diagnostics (Mannheim, Germany). In every single experiment, each concentration was tested in four replicates and each experiment has been repeated in at least three independent biological repeats ($n = 3$ for LDH assays of mixed cortical cells, $n = 6$ for WST-1 assay of mixed cortical cells, $n = 3$ for LDH assays of neuronal-enriched cells, and $n = 3$ for LDH assay of astrocytes). Mean values of the experimental repeats ± SEM are given. Calculation of mean values, SD, and SEM was done in Excel. Statistical analysis of the data was done in SPSS (SPSS 12.0, IBM). A multivariate ANOVA (MANOVA) was performed. In parallel, we compared each data group to each other data group directly with Student's *t*-test.

Cell lysates, SDS-PAGE, immunoblot, and detection of protein carbonyls. Cells were washed with PBS several times and lysed by adding a modified radioimmunoprecipitation assay buffer (50mM Tris/HCl, pH 7.4; 150mM NaCl, 1mM EDTA, 1% Igepal, and 0.25% Na-deoxycholate). Cell lysates were centrifuged with 16,800 × g at 4°C in a table top centrifuge (Eppendorf) and stored at −80°C. Protein concentrations were determined through Bradford assay (Bio-Rad, Munich, Germany), and SDS-PAGE was performed according to standard protocols. In each lane, 20 µg total protein was loaded and 10% SDS-PAGE gels were used. SDS-PAGE gels were transferred onto nitrocellulose membranes with a semidry blotting system. For detection of protein carbonyls, OxyBlot Kit (Millipore, Schwalbach, Germany) was used according to manufacturer's instructions. In addition, Western blots were performed with antibodies against heme oxygenase-1 (HO-1), tubulin, or actin (Abcam, Cambridge, U.K.). All primary antibodies were used in a 1:1000 dilution with overnight incubation. Secondary antibodies were obtained from Dianova (Hamburg, Germany) and used in a dilution between 1:10,000 and 1:20,000. Enhanced chemiluminescence reagent was obtained from Pierce ThermoFisher Scientific (Bonn, Germany) and used according to manufacturer's instructions. Immunoblots were documented with a GelDoc system (Bio-Rad) and analyses were performed with QuantityOne software (Bio-Rad).

Calcium responses. Cells were used after 2 weeks of differentiation *in vitro*. The measurement was performed according to a protocol published earlier (Kahlert *et al.*, 2005). Briefly, the cells were preincubated with 2µM Fura-2/AM (Molecular Probes via MoBiTec, Goettingen, Germany) in NaHBS (HEPES buffered saline solution: 145mM NaCl, 5.4mM KCl, 1.8mM $CaCl_2$, 1mM $MgCl_2$, 25mM glucose, and 20mM HEPES/Tris, pH 7.4) for 30 min. After washing of cells, the nanoparticles were added and then calcium responses were monitored immediately by measuring the 340/380 nm ratio at single cell level. Fluorescence intensity was recorded alternately at 340 and 380 nm excitation and 520 nm emission with a Zeiss Axiovert microscope (40×/1.30 oil immersion objective) and a fluorescence imaging system from TILL Photonics (Graefelfing, Germany). For data analysis, the fluorescence ratio R ($R = \Delta F_{340}/F_{380}$) at the two wavelengths, 340 and 380 nm, was measured for each cell individually. In one experiment, we analyzed between 30 and 80 individual cells. Each experiment has been performed at least in three independent biological repeats. For data analysis, the fluorescence ratios have been exported to Excel. They have been normalized (starting point at beginning of the measurement was set to 1) such that we could compare between individual experiments. For quantification, the areas under the curves (AUCs) have been calculated. In each experiment, we calculated the AUC for each cell separately and calculated a mean value, a SD, and an SEM for each dose group in each experiment. Finally, from the independent repeats, we calculated the mean values for the AUC, the SD, and SEM. This analysis has been done in Excel. Statistical analysis has been performed in Excel (Student's *t*-test) and in SPSS (MANOVA).

Reactive oxygen species measurement in live cells. Mixed primary cortical cells were used after 2 weeks of differentiation *in vitro*. Reactive oxygen species (ROS) measurement was performed with dihydroethidium (DHE) dye (Molecular Probes via MoBiTec) as published elsewhere (Kahlert *et al.*, 2005). Briefly, the cells were preincubated with the nanoparticles for 1 h. Afterward, 1µM DHE in NaHBS (HEPES buffered saline solution: 145mM NaCl, 5.4mM KCl, 1.8mM $CaCl_2$, 1mM $MgCl_2$, 25mM glucose, and 20mM HEPES/Tris pH 7.4) was added for 30 min. After washing of cells, ROS generation was immediately monitored at 520 nm at a single cell level. In one experiment, we analyzed between 30 and 80 individual cells. Each experiment has been performed at least in three independent biological repeats. For data analysis, the fluorescence values at 520 nm have been exported to Excel. The slope of the response curve has been determined from the values at 15 min after starting the measurement and from the onset of the measurement. In one experiment, we determined the response of each cell separately and calculated the mean response (mean of the slopes), the SD, and SEM in Excel. Finally, from at least three independent experiments, we determined the mean values, the SD, and the SEM. Statistical analysis has been performed in Excel (Student's *t*-test) and in SPSS (MANOVA).

Downloaded from http://toxsci.oxfordjournals.org/ at Bundesinstitut fuer Gesundheitlich on July 24, 2014

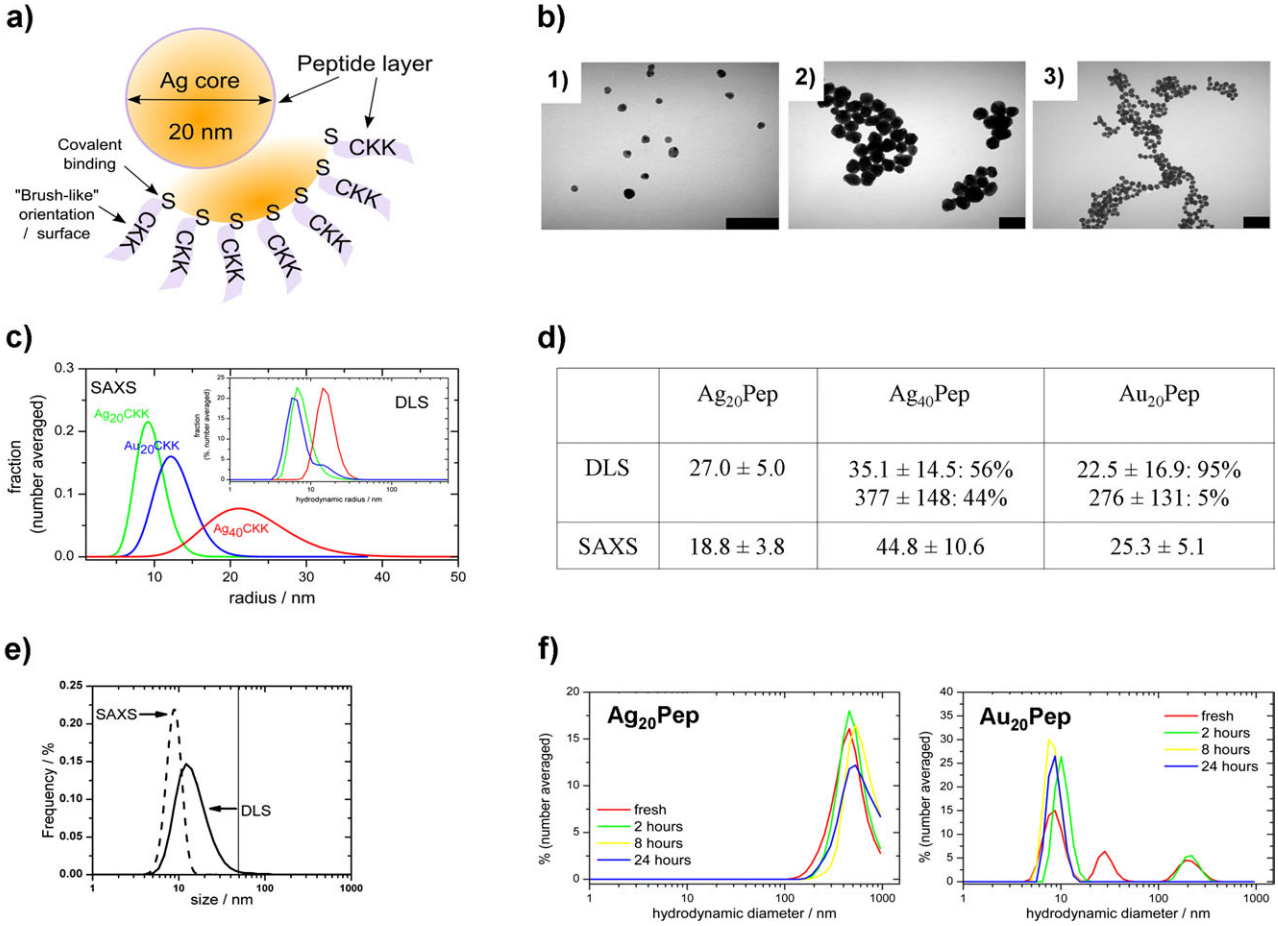

	Ag_{20}Pep	Ag_{40}Pep	Au_{20}Pep
DLS	27.0 ± 5.0	35.1 ± 14.5: 56% 377 ± 148: 44%	22.5 ± 16.9: 95% 276 ± 131: 5%
SAXS	18.8 ± 3.8	44.8 ± 10.6	25.3 ± 5.1

FIG. 1. Characterization of nanoparticles. (a) Schematic representation of the peptide-coated SNP applied in this study. (b) Representative TEM images of peptide-coated 20 nm SNP (Ag_{20}Pep, 1), peptide-coated 40 nm SNP (Ag_{40}Pep, 2), and peptide-coated 20 nm GNP (Au_{20}Pep, 3). Scale bars are shown in black (100 nm). (c) Analysis of nanoparticles suspension (H_2O) by light scattering (DLS) and SAXS to demonstrate the size distribution. (d) Summary of the DLS and SAXS analyses (H_2O) of nanoparticles. For DLS, number-averaged hydrodynamic diameters are reported (in nanometer). For SAXS, diffraction curves were fitted using Schulz sphere distribution. (e) Direct comparison of DLS and SAXS curves for Ag_{20}Pep. (f) Analysis of Ag_{20}Pep and Au_{20}Pep suspension in cell culture medium over time to characterize the nanoparticles as they were used in the experiments.

TEM analysis. TEM analysis was performed as previously described (Richardson *et al.*, 1960). Cells in the culture dish were washed with PBS and fixed overnight by immersion with Karnovsky's fixative at 4°C. After three washes in 0.1M cacodylate buffer, post-fixation was performed with 2% osmium tetroxide in 0.1M cacodylate buffer for 1 h at 4°C. After another three washes in 0.1M cacodylate buffer, cells were removed from the culture dish and centrifuged at 2000 × g for 5 min. The pellet was then coated with 1.5% agar (Merck Eurolab, Darmstadt, Germany) for 30 min at 4°C. Subsequently, the agar with the attached cell layer was removed from the wells. The samples were then dehydrated in an ascending ethanol series (30–100% alcohol vol/vol) and embedded in Epon using beem capsules (Plano, Marburg, Germany). Polymerization was carried out at 60°C for 24 h. Semithin sections (1 µm) were cut on an Ultracut E ultramicrotome (Reichert-Jung, Vienna, Austria) with a diamond knife, stained as published elsewhere (Richardson *et al.*, 1960), and analyzed by light microscopy. Ultrathin sections (60 nm) were cut with a diamond knife, mounted on copper grids (Plano), and examined with a Zeiss 10CR electron microscope (Jena, Germany). We did not perform post-fixation with lead citrate and uranyl acetate, which often is associated with the occurrence of osmium artifacts.

Morphological assessment by immunofluorescence. Cells were treated with 10 or 20 µg/ml Ag_{20}Pep or 20 µg/ml Au_{20}Pep particles for 24 h and after three washing cycles, they were fixed with 4% paraformaldehyde for 20 min. For the staining of neurons and astrocytes, we used antibodies against synaptotagmin (presynaptic marker) obtained from Sysy (Göttingen, Germany), NeuN (neuronal marker) obtained from Millipore (Schwalbach, Germany), and glial fibrillary acidic protein (GFAP) obtained from Roche Diagnostics (Mannheim, Germany), respectively, as published elsewhere (Kahlert *et al.*, 2005).

RESULTS

Synthesis and Characterization of Silver Nanoparticles

In this study, we used SNP that have been stabilized through covalent peptide coating based on the short sequence CKK (Fig. 1a). We previously described the synthesis and characterization of these particles (Graf *et al.*, 2009). As a biomimetic approach, our system offers several advantages. First, synthesis conditions can be kept mild and without organic solvents, thus avoiding residual traces of organics that later might interfere with the bioassay. Second, the peptide acts as a strong structure- and size-directing agent and thus, we obtained very homogenous

Downloaded from http://toxsci.oxfordjournals.org/ at Bundesinstitut fuer Gesundheitlich on July 24, 2014

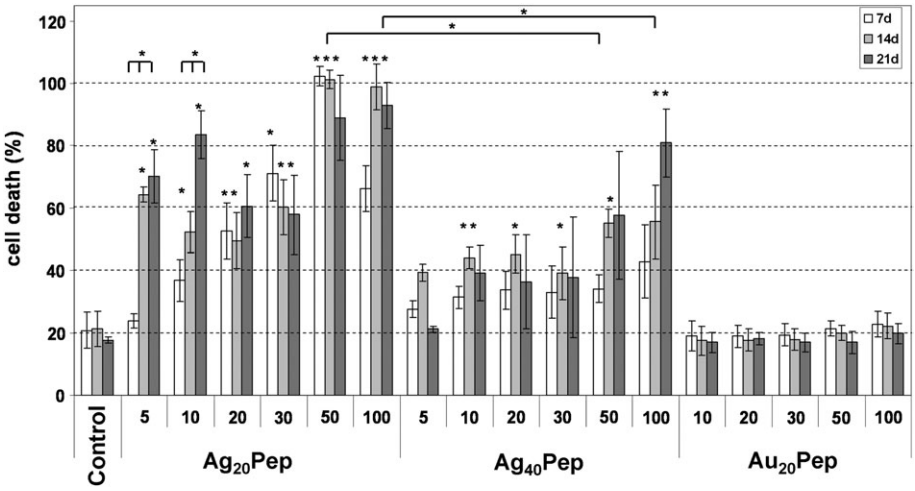

FIG. 2. Dose-, size-, and differentiation-dependent toxicity of different nanoparticles in primary mixed neural cell cultures. Cytotoxicity of the following nanoparticles was tested via LDH viability assay after 24 h of exposure: 20 nm SNP (Ag_{20}Pep), 40 nm SNP (Ag_{40}Pep), and 20 nm GNP (Au_{20}Pep). In each experiment, four replicates per concentration were tested. The experiment was repeated three times. The data shown are mean values of three independent experiments (±SEM). For statistical analysis, the whole data set was analyzed with a MANOVA. In parallel, all groups have been compared individually with each other with a Student's *t*-test. Significance is indicated by an asterisk.

narrow-sized nanoparticles of well-defined material properties (e.g., polydispersity index of 0.18; values of > 0.3 are regularly achieved by classic citrate-based reductive synthesis). In this study, we used two different SNP with a diameter of 20 nm (Ag_{20}Pep) or 40 nm (Ag_{40}Pep). GNP of 20 nm diameter with the same coating (Au_{20}Pep) were used for comparison. The nanoparticles were extensively characterized after synthesis via a set of different techniques as described (Graf *et al.*, 2009). TEM pictures of all nanoparticles are depicted in Figure 1b. The suspensions were characterized by DLS and SAXS; the size distribution of all nanoparticles is depicted in Figure 1c. The table in Figure 1d summarizes the results of the DLS and SAXS measurements. One obvious difference between the DLS and SAXS measurement is the slightly different size of the particles as it becomes obvious for Ag_{20}Pep in Figure 1e. DLS measures the hydrodynamic radius of the particle, the coat, and the hydrate shell, whereas in SAXS, only the electron dense particle core has been analyzed. Thus, from the difference, one can estimate the size of the coat and the hydrate shell. Finally, we characterized the agglomeration behavior of the particles after being transferred into cell culture medium (Fig. 1f).

Cytotoxicity of Silver Nanoparticles

In these experiments, we used mixed primary cortical neural cells. These cultures mainly consist of neurons and astrocytes but also contain a low number of oligodendrocytes. This cell culture system has been carefully established and characterized. Prior to treatment, cells were kept in culture for 7, 14, and 21 days, respectively. In 7-day-old cultures, the neurons already started to form axons and dendrites, but the formation of functional synapses had only begun. In 14-day-old cultures, synaptic contacts were present and functional networks became established. Twenty-one-day-old cultures appeared further matured with higher degrees of intercellular connections, as observed by immunofluorescence staining. Development of rat cortical neuronal networks *in vitro* has been described in detail elsewhere (Robinette *et al.*, 2011). SNP-dependent effects on cell viability and cytotoxicity were assessed after 24 h of incubation by applying both the WST-1 and the LDH assay in parallel. Both toxicity assays have been optimized to reduce potential particle interferences and both delivered similar results. Results of the LDH assay are shown in Figure 2. The WST data, which yield similar results, are given in Supplementary figure 1. For the smaller Ag_{20}Pep particles, we observed strong cytotoxicity. The larger Ag_{40}Pep were much less toxic at all concentrations tested if doses were compared on a mass basis. We tested whether the differences in cytotoxicity of Ag_{20}Pep and Ag_{40}Pep particles were statistically significant with Student's *t*-test for each of the 7-, 14-, and 21-day cultures separately and found statistically significant differences for the two highest test concentrations (50 and 100 μg/ml). By contrast, GNP did not show any significant toxicity compared with control cells. Because the cytotoxicity curves displayed a rather complex dependence on the concentration applied, the calculation of reliable IC(50) values was unfeasible. Furthermore, we were interested whether the 7-, 14-, and 21-day cultures would display a different response upon nanoparticle treatment. For this purpose, we first performed a MANOVA and found statistically significant differences for the low-dose treatment groups of Ag_{20}Pep (5 and 10 μg/ml). This was confirmed by Student's *t*-test. With increasing time in culture and thus with increasing degree of differentiation, the cultures displayed stronger SNP-mediated toxicity. This result points to a greater vulnerability of cells at later differentiation stages. In the higher dose range (50–100 μg/ml), no detailed conclusions can be drawn from the dose-response dependence observed; the toxicity

Downloaded from http://toxsci.oxfordjournals.org/ at Bundesinstitut fuer Gesundheitlich on July 24, 2014

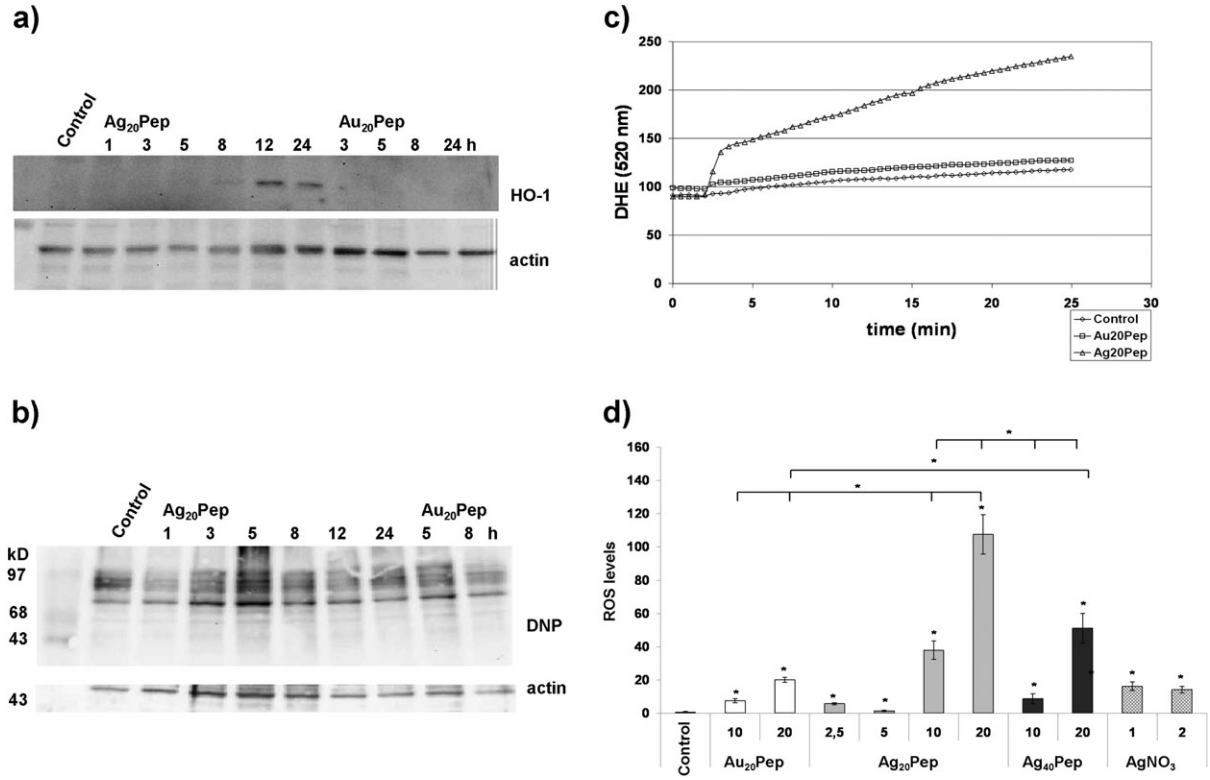

FIG. 3. Generation of oxidative stress in primary neural cells by nanosilver. (a) Time-dependent induction of HO-1 expression in primary mixed neural cells treated with 20 μg/ml Ag_{20}Pep particles (incubation times: 1–24 h); Au_{20}Pep particles at 20 μg/ml served as control (incubation time: 3–24 h). (b) Time-dependent formation of protein carbonyls in primary mixed neural cells after treatment with 20 μg/ml Ag_{20}Pep particles (incubation time: 1–24 h); Au_{20}Pep particles at 20 μg/ml served as control (incubation time: 5 and 8 h). Protein carbonyls are visualized as 2,4-dinitrophenyl hydrazone (DNP) adducts. (c) Measurement of ROS with DHE dye in single live cells upon treatment with 10 μg/ml Au_{20}Pep or 10 μg/ml Ag_{20}Pep particles. Particles were preincubated for 1 h with the cells before the measurement was started. Control: no nanoparticles added. (d) Quantification of ROS formation. The values represent the slope of the response curves. In each experiment, between 30 and 80 individual cells have been analyzed. Each experiment was repeated at least three times. Mean values from at least three experiments with SEM are shown. For analysis of significance, a MANOVA and Student's *t*-tests were done. Significant differences are marked with an asterisk. For comparison, ionic silver ($AgNO_3$) was applied at 1 and 2μM. Particle concentrations are given in micrograms per milliliter.

was very high regardless of the differentiation state. If doses were compared based on the surface area of the nanoparticles, the cytotoxicity of Ag_{20}Pep and Ag_{40}Pep largely appears similar (Supplementary fig. 2).

In addition, we separately tested the individual cell types that were present in the mixed cultures. To this end, neurons were enriched by treating of the cultures with AraC, a compound that selectively eliminates proliferating astrocytes (Manev *et al.*, 1991). In the resulting cultures that contained more than 95% neuronal cells, particle-mediated toxicity was assessed with LDH-1 assay (Supplementary fig. 3a). Control cell death was already relatively high, thus indicating a significant level of neuronal demise under control conditions. At particle concentrations of up to 30 μg/ml Ag_{20}Pep, no additional effect could be detected. Only at 50 μg/ml, the cytotoxic effect of Ag_{20}Pep on the neuronal-enriched cultures was statistically significant. Astrocytes purified from total brain and transferred into culture are free of neurons but do contain some oligodendrocytes and microglial cells. These cultures contain more than 90% astrocytes. Ag_{20}Pep-mediated cytotoxicity assessed with LDH-1 assay revealed a dose dependency (Supplementary fig. 3b). Concentrations as low as 5 μg/ml already had a detectable effect, and 10 μg/ml induced a significant effect, indicating that this cell type is much more vulnerable against SNP when compared with neurons. GNP again proved inert.

Silver Nanoparticles Cause Oxidative Stress

SNP-mediated oxidative stress responses in cells were demonstrated via two different endpoints (Fig. 3). First, we analyzed the induction of HO-1, which is a well-established marker of chemical-induced oxidative stress, and followed the kinetics of HO-1 induction (Fig. 3a), which was first detectable 8 h after treatment.

We then demonstrated the generation of ROS. Because most ROS formed in cells are being scavenged by proteins, oxidative protein modifications such as protein carbonyls can serve as a sensitive indirect endpoint of ROS formation in cells. We found strong formation of protein carbonyls in our cultures upon SNP exposure (Fig. 3b), detectable already at 3 h after initial treatment. By contrast, GNPs were not effective. We

Downloaded from http://toxsci.oxfordjournals.org/ at Bundesinstitut fuer Gesundheitlich on July 24, 2014

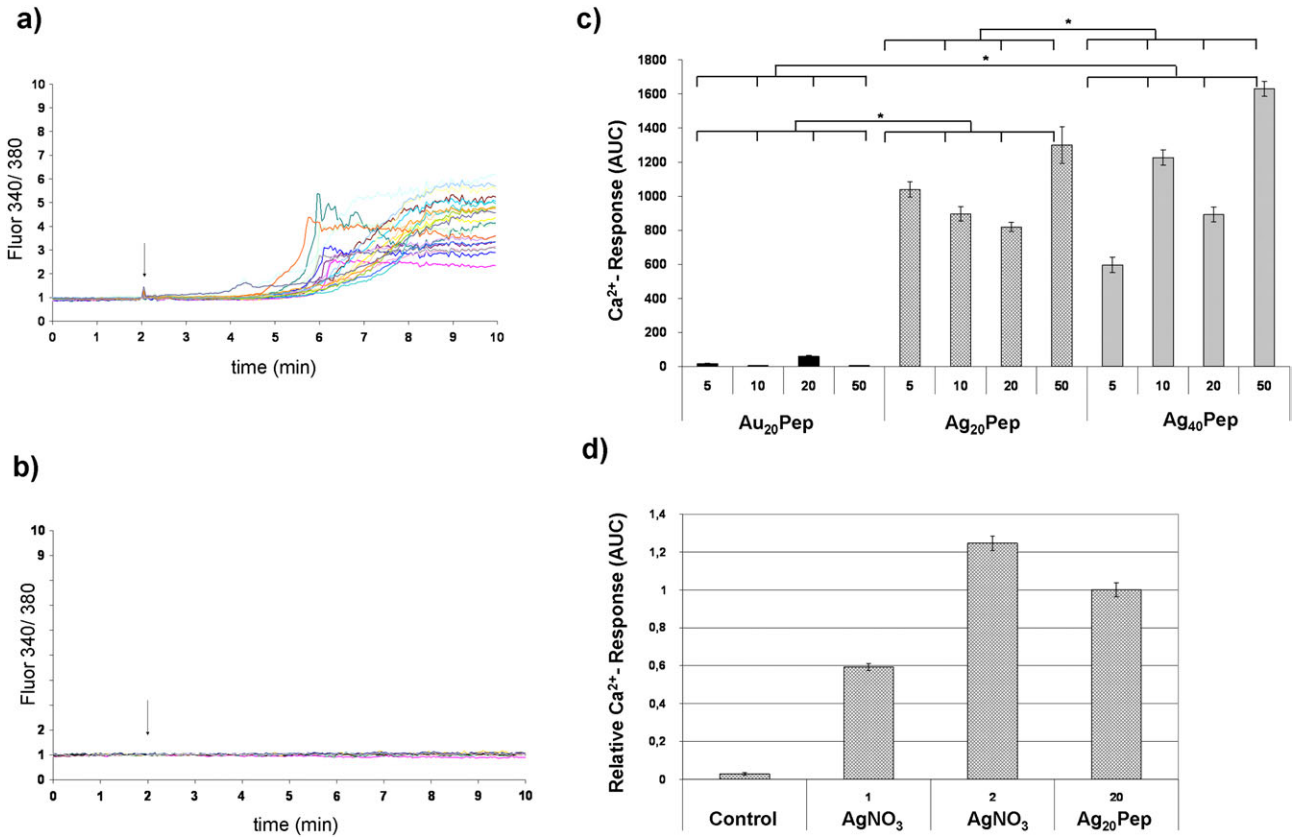

FIG. 4. Acute calcium responses of nanosilver in primary neural cells. The time-dependent calcium increase was monitored with the Fura-2AM indicator dye. The arrow depicts the time point when nanoparticles were added to cells. (a) Calcium response in cells after addition of 10 μg/ml Ag_{20}Pep particles. (b) Calcium response in cells after addition of 10 μg/ml Au_{20}Pep particles. (c) The calcium responses were quantified by calculating the AUC. In each experiment, between 30 and 80 individual cells are followed. Each experiment was repeated at least three times. Given are mean values from at least three individual experiments with SEM. Particle concentrations are given in micrograms per milliliter. Significance has been calculated with a MANOVA and with Student's *t*-tests. Significant differences are marked with an asterisk. (d) For comparison, ionic silver as $AgNO_3$ (1 and 2μM) was tested. Again, in each experiment, between 30 and 80 cells are measured. Each experiment was repeated three times. AUC were calculated. Shown are the AUC mean values with SEM in relation to the response obtained after treatment with 20 μg/ml Ag_{20}Pep particles (set as 1).

have recently demonstrated that treatment with SNP leads to induction of HO-1 and formation of protein carbonyls in a macrophage cell line model (Haase *et al.*, 2011). Quantitative data of the results described in Figures 3a and 3b are provided in Supplementary figure 4.

We also monitored the formation of ROS directly in living cells by applying the indicator dye DHE (Fig. 3c). Cells were preincubated with SNP or GNP for 1 h and then analyzed. After shorter preincubation time (e.g., 15 min of preincubation) or directly after addition of the nanoparticles, we were unable to detect any ROS formation (Supplementary fig. 5). After 1 h of preincubation, however, SNP led to a steady increase in ROS levels, although the effects of GNP were very low in comparison. If cells were pretreated with an antioxidant (NAC), ROS formation could not be measured anymore (see below). For comparison, we included ionic silver (solution of 1 and 2μM $AgNO_3$). We assume that these concentrations of ionic silver would rather exceed the amount of ionic silver being released from the SNP. As our SNP are tightly coated with a covalent peptide layer, we actually do not expect any significant dissolution. Ionic silver produced only a minimal amount of ROS, which was comparable to the response measured with the GNP (Fig. 3d).

Comparison of the concentration-dependent effects of SNP on cellular ROS levels again revealed that smaller particles cause significantly stronger effects if the same mass doses are being considered.

Silver Nanoparticles Evoke an Acute Calcium Response

After treatment of mixed neural cells with SNP, we observed a fast and strong intracellular calcium response. This response usually was observed within 3–6 min after addition of the SNP (Fig. 4a). Conversely, GNP did not induce such a calcium response (Fig. 4b). We found a calcium rise after treatment with SNP in the concentration range of 5–50 μg/ml. To compare the different responses, the AUCs have been calculated. Mean values from at least three individual experiments (each with 30–80 analyzed cells) have been compared. For statistical analysis, we performed a MANOVA and Student's *t*-test.

Downloaded from http://toxsci.oxfordjournals.org/ at Bundesinstitut fuer Gesundheitlich on July 24, 2014

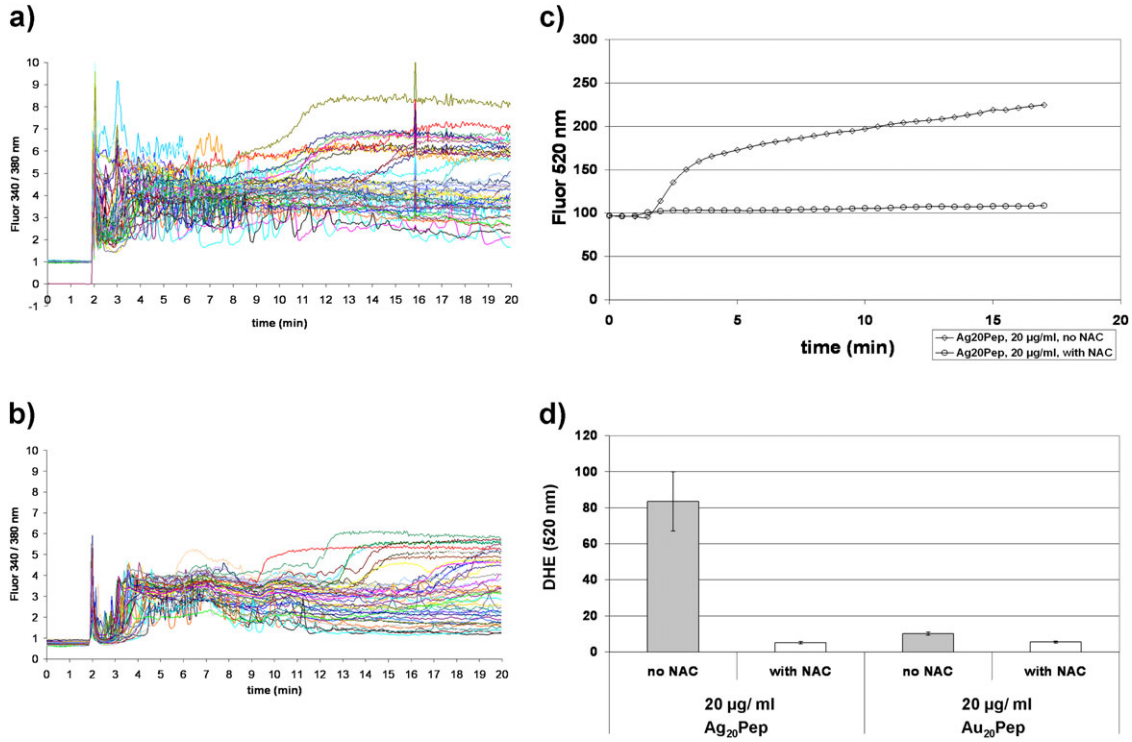

FIG. 5. Effects of antioxidant pretreatment on nanoparticle-induced ROS generation and calcium responses. The primary neural cultures were used without and with pretreatment with NAC (final concentration 10mM, 1 h). The calcium increase was monitored with the Fura-2AM indicator dye. The nanoparticles were added to cells after 2 min. (a) Calcium response after addition of 20 µg/ml Ag_{20}Pep particles without NAC pretreatment. (b) Calcium response after addition of 20 µg/ml Ag_{20}Pep particles with NAC pretreatment. (c) Measurement of ROS was performed with DHE dye in a single live cell upon treatment with 20 µg/ml Ag_{20}Pep particles without or with NAC pretreatment. (d) Quantification of ROS formation (from graph in Fig. 5c together with data for nanogold). Mean values of at least 30 individual cells in one representative experiment, including SEM, are shown. Each experiment has been repeated three times.

Unexpectedly, both types of SNP were able to induce a strong, acute calcium response, which was significantly stronger compared with Au_{20}Pep applied at same doses (Fig. 4c). The dose dependency was rather unusual. Already at 5 µg/ml Ag_{20}Pep, we detected a strong calcium response, which was further decreasing with increasing concentrations. At the cytotoxic dose of 50 µg/ml SNP, the calcium levels measured were again increasing. However, at the lowest concentration (5 µg/ml) tested, the Ag_{20}Pep particles provoked a much stronger response compared with Ag_{40}Pep particles. For comparison, we included ionic silver at concentrations of 1 and 2µM (Fig. 4d). The response was calculated as AUC in relation to the response of 20 µg/ml Ag_{20}Pep. We found a significant calcium signal for ionic silver as well, which was in a comparable range to the calcium signals obtained with 20 µg/ml Ag_{20}Pep.

Neuronal-enriched cultures (> 95% neurons) also responded with strong increases of intracellular calcium, indicating that neurons are susceptible to SNP (Supplementary fig. 6). However, at cytotoxic SNP concentrations (50 µg/ml), calcium responses in neurons completely disappeared (Supplementary fig. 6b). We also tested astrocyte cultures separately and found calcium responses as well (data not shown). Our aim at this stage was not to compare nor quantify the responses obtained in neuronal versus astrocyte cultures. Based on the results obtained, however, we are sure that both cell types can respond to nanosilver treatment with increasing intracellular calcium levels.

Pretreatment of the mixed cultures with the antioxidant NAC had no effect on the calcium signals, although the formation of ROS could be prevented (Fig. 5). This indicates that the cellular redox state is of only minor importance for the neuronal calcium signal induced by SNP.

Silver Nanoparticles Are Mainly Taken up by Astrocytes

To analyze the uptake and the intracellular distribution, we performed ultrastructural analysis with TEM. In order to differentiate, we tested each cell type separately. We prepared astrocyte cultures and neuronal-enriched cultures and treated them with 10 µg/ml Ag_{20}Pep for 24 h. When analyzing the astrocyte culture, we frequently detected cells that had incorporated SNP (Fig. 6a). Typically, within one cell, we could find several large clusters of nanoparticles (arrows in Fig. 6a). We did not observe individual nanoparticles freely dispersed inside those cells. A larger magnification of the particles inside astrocytes is shown in Supplementary figures 7a and 7b. The nanoparticles could be detected in cellular compartments, most likely lysosomes. The other cellular

Downloaded from http://toxsci.oxfordjournals.org/ at Bundesinstitut fuer Gesundheitlich on July 24, 2014

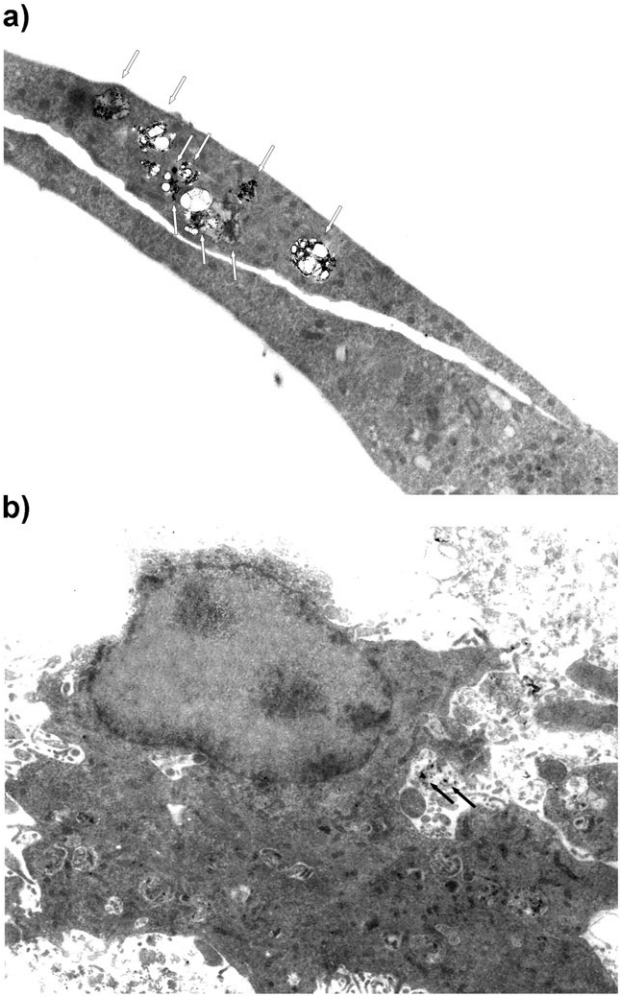

FIG. 6. Analysis of nanoparticle uptake with TEM. (a) A representative image obtained from an astrocyte culture treated with 10 μg/ml Ag_{20}Pep for 24 h. Frequently, cells contained large agglomerates of SNP, as depicted by arrows. Magnification 5000×. (b) A representative image obtained from a neuronal-enriched culture treated with 10 μg/ml Ag_{20}Pep for 24 h. Typically, cells do not contain any SNP agglomerates. Occasionally, individual particles or small agglomerates of SNP can be found (arrows). Magnification 3150×.

organelles (e.g., nuclei, mitochondria, ER) did not contain nanoparticles. For the neuronal-enriched cultures (Fig. 6b), the outcome was different. Most of the cells were free of nanoparticles. Only some cells could be found that contained nanoparticles. Inside the neurons, we never detected the same amount of large clusters as in astrocytes but much smaller aggregates (arrows in Fig. 6b). For some of these SNP aggregates, it is even uncertain whether they are really incorporated inside cells as we typically detected them in areas outside the main cell body.

Silver Nanoparticles Strongly Affect the Morphology of Astrocytes

After 24 h of treatment, the mixed neural cells were fixed and immunostained with markers for neurons and astrocytes to follow morphological changes. Untreated cells, cells treated with 10 or 20 μg/ml Ag_{20}Pep, and 20 μg/ml Au_{20}Pep particles are shown in Supplementary figure 8. Neurons are stained with synaptotagmin-1 and NeuN (shown in red) and astrocytes are stained with GFAP (shown in green). In control cultures (no treatment), neurons form dense networks with nicely visible dendrites. Astrocytes also show typical cell body extensions (Supplementary fig. 8a). Upon treatment with low doses of SNP (i.e., 10 μg/ml), astrocytes become grossly morphologically disorganized, whereas the neurons appear similar as in controls, thus still forming dense networks with dendrites (Supplementary fig. 8b). However, at higher SNP concentration (i.e., 20 μg/ml), both cell types become affected (Supplementary fig. 8c). GNPs again are without effect (Supplementary fig. 8d).

DISCUSSION

The results presented here demonstrate that SNP adversely affect primary neural cells when applied at moderate concentrations. Both types of SNP could induce significant cytotoxicity with a clear dose dependency. The effects of the smaller Ag_{20}Pep particles compared with the larger Ag_{40}Pep particles were stronger when doses are considered according to their mass. However, it appeared difficult to calculate IC(50) values. For the low-dose range (5 and 10 μg/ml SNP), we observed statistically significant differences between the 7-, 14-, and 21-day cultures as the further differentiated neural cells were more vulnerable toward SNP. In the high-dose range, the particles were toxic regardless of the differentiation state of the cultures.

For cytotoxicity testing, we included concentrations of up to 100 μg/ml. For the tests addressing the mechanism of action, we used 5–20 μg/ml, which equals 2.5–10 μg/cm^2 or 0.05–0.2 ng per cell (the metal content of the nanoparticles was ~95%), thus representing a relatively low to medium concentration range for *in vitro* tests. In this concentration range, we observed maximal oxidative stress responses and acute calcium signals. To evaluate the doses applied, the following considerations need to be taken into account. Other *in vitro* studies with primary neural cells used similar or even higher concentrations of nanoparticles, e.g., up to 300 μg/cm^2 of carbon black or titanium dioxide (Gramowski *et al.*, 2010). Zhaowei *et al.* (2009) used SNP and detected effects at 10 μg/ml, as did Liu *et al.* (2011). A few *in vitro* studies analyzed the translocation of SNP through and accumulation in the BBB. In these studies, up to 50 μg/ml (Trickler *et al.*, 2010) or 100 μg/ml SNP (Tang *et al.*, 2010) were used. Based on these data, we believe that the concentrations tested in the present study are of reasonable range for an *in vitro* study.

Nevertheless, compared with *in vivo* studies, the applied doses are high. In general, *in vitro* studies rather represent worst-case scenarios and are therefore useful for the testing of acute toxicity. Typically, in *in vitro* studies, one single dose is

Downloaded from http://toxsci.oxfordjournals.org/ at Bundesinstitut fuer Gesundheitlich on July 24, 2014

being applied, whereas in *in vivo* studies, particles are usually being delivered over a longer time period. To compare our study design and the obtained results with the expected or estimated situation *in vivo*, we refer to the 4-week inhalation study in rats conducted by Ji *et al.* (2007). The authors used nanosilver with a mean diameter of 12–15 nm in a low, a medium, and a high dosage group. Only at high dosages, the authors could observe any effect. The total delivered doses in terms of particle number per animal in this group were 1.47×10^{12} (female) and 2.16×10^{12} (male), which equals 68 μg (female) and 101 μg (male) nanosilver, respectively. Data for SNP are not available, but for other types of nanoparticles such as polystyrene nanoparticles, it is known that roughly 80% of the instilled dose will be retained in the lungs (Oberdörster, 2005). However, under healthy conditions *in vivo*, only a very small fraction (less than 1 or 2%) of the particles delivered may reach the brain (Ji *et al.*, 2007). This would equal 3.45×10^{10} particles or less. In our *in vitro* study, we started to observe effects at 5–10 μg/ml (2.5–5 μg/cm^2) SNP, which equals to 1.1 to 2.4×10^{11} particles per assay.

Under certain pathological conditions (e.g., infections such as meningitis, stroke, or systemic inflammation), it is well described that the BBB function can be compromised. Because the numbers of nanoparticles translocated into the brain may significantly increase, risk assessors also have to consider the corresponding tissue exposures under such conditions. However, only rarely, this issue has been addressed in the literature. Rousseau *et al.* (1997) investigated the translocation of iron oxide nanoparticles into the brain of rats after disruption of the BBB. The authors observed an increase in the particle uptake of 160–290%. These results demonstrate that under certain conditions, a tremendous increase of nanoparticle uptake into the CNS can be expected.

Intracellular formation of ROS was measured directly by applying an indicator dye as well as indirectly via cellular follow-up products, such as protein carbonyls. In addition, induction of the HO-1 protein indicated the presence of oxidative stress. All these responses followed a different time course, thereby possibly mirroring a hierarchical progression of cellular oxidative stress responses. ROS are detectable early, but cells need to be preincubated with SNP for 1 h. ROS formation could not be detected as an acute response or after only short preincubation time of 15 min. The formation of protein carbonyls was first detectable about 3 h after starting the treatment, thus being an early oxidative stress marker. By contrast, the induction of cytoprotective enzymes, such as HO-1, requires the activation of transcription factors and is therefore detectable rather late, beginning at 8 h after treatment. The levels of protein carbonyls reached a peak value at around 5 h after starting the exposure and subsequently decreased at prolonged incubation times.

For neural cells, the oxidative stress response is of particular interest because chronically increased levels of ROS have been associated with neurodegenerative disorders, such as Alzheimer's and Parkinson's disease (Smith and Wayne, 2007; Sompol *et al.*, 2008). A striking example that nanoparticle-mediated effects in the CNS may entail clinical consequences comes from the observation that high levels of manganese oxide nanoparticles, generated in welding processes, can be linked to the development of a special kind of Parkinsonism observed in welders several years after respiratory exposure (Bowler *et al.*, 2006). As shown in rats, manganese oxide nanoparticles are translocated into the brain after inhalation. Particles could be detected in the olfactory bulbs and in other parts of the brain, such as cortex or striatum (Elder *et al.*, 2006).

Upon exposure to SNP, we also observed a strong acute calcium signal in neural cell cultures, which appeared within minutes after nanoparticle addition. Thus, this calcium signal could be detected before any other response became measurable. Given this, it seems unlikely that the calcium signal results as consequence of ROS formation. To prove this further, we completely blocked the formation of ROS by pretreatment of cells with NAC. Even under these conditions, the calcium signals could still be measured. Additionally, the calcium signals seem to decline with increasing SNP concentrations. This u-shaped dose-response curve might be considered rather unusual. Interpretations for this occurrence would be highly speculative at the moment. However, in neurotoxicology, several such u-shaped dose-response curves have been reported (see review in Davis and Svendsgaard, 1990). Ionic silver was able to induce an acute calcium response as well—in a range comparable to the lowest effect obtained with Ag_{20}Pep particles. By contrast, the silver ion–induced ROS formation was significantly lower compared with the effect triggered by SNP. Taken together, based on our data, it seems unlikely that both processes are mechanistically linked to each other. The data presented further suggest that SNP can interfere with calcium-mediated signaling processes of neural cells and thus might also affect neural signal transduction processes once becoming bioavailable in the CNS tissue. Recently, it has been demonstrated that the electric activity in primary murine cortical networks becomes altered during exposure to nanoparticles, such as carbon black, hematite, and titanium dioxide (Gramowski *et al.*, 2010).

When testing the effects on the cell types individually, we found astrocytes being highly vulnerable toward SNP treatment, although neurons were affected only at higher concentrations. This could be concluded from the cytotoxicity tests with neuronal- or astrocyte-enriched cultures. In good agreement with this, we find that astrocytes effectively incorporate SNP, although only few of them were detectable in neuronal cells under similar conditions. In addition, in immunofluorescence studies of mixed cultures, mainly the astrocyte morphology was found altered at lower concentrations (10 μg/ml). For this cell type, extensions disappeared and only the cell soma remained visible. Only at 20 μg/ml SNP did both cell types show an equally affected morphology. This finding is of special interest as the particular role of astrocytes in several neurodegenerative diseases has been

Downloaded from http://toxsci.oxfordjournals.org/ at Bundesinstitut fuer Gesundheitlich on July 24, 2014

intensely discussed, and it seems likely that this cell type is being initially affected during pathogenesis (Maragakis and Rothstein, 2006). The high vulnerability of astrocytes toward nanoparticle exposure, as demonstrated here, might thus have fundamental consequences on the proper function of neural networks. Further studies are needed to analyze this in more detail.

CONCLUSIONS

Our data suggest that SNP affect functional processes in neuronal networks. Depending on the bioavailability of the particles *in vivo*, long-term exposure against low doses of SNP might trigger adverse effects in the CNS. Further studies are needed to understand the underlying molecular mechanisms and the physiological consequences.

SUPPLEMENTARY DATA

Supplementary data are available online at http://toxsci.oxfordjournals.org/.

FUNDING

Financial support by the Federal Land Sachsen Anhalt (CBBS Project C1), the Federal Ministry of Food, Agriculture and Consumer Protection (BMELV), the Federal Institute for Risk Assessment (BfR), the Federal Institute for Materials Research and Testing (BAM), the Swiss National Science Foundation, the NCCR-Nanosciences, the Free University, the University of Potsdam, and the MPI of Colloids and Interfaces is gratefully acknowledged. A. Mantion thanks the Adolf-Martens e.V. for an Adolf-Martens Fellowship.

ACKNOWLEDGMENTS

The authors acknowledge the excellent technical assistance of Evelyn Busse and Abidat Schneider.

REFERENCES

Arora, S., Jain, J., Rajwade, J. M., and Paknikar, K. M. (2008). Cellular responses induced by silver nanoparticles: In vitro studies. *Toxicol. Lett.* **179,** 93–100.

Bowler, R. M., Koller, W., and Schulz, P. E. (2006). Parkinsonism due to manganism in a welder: Neurological and neuropsychological sequelae. *Neurotoxicology* **27,** 327–332.

Carlson, C., Hussain, S. M., Schrand, A. M., Braydich-Stolle, L. K., Hess, K. L., Jones, R. L., and Schlager, J. J. (2008). Unique cellular interaction of silver nanoparticles: Size-dependent generation of reactive oxygen species. *J. Phys. Chem. B* **112,** 13608–13619.

Chen, D., Xi, T., and Bai, J. (2007). Biological effects induced by nanosilver: In vivo study. *Biomed. Mater.* **2,** S126–S128.

Chen, J., Tan, M., Nemmar, A., Song, W., Dong, M., Zhang, G., and Li, Y. (2006). Quantification of extrapulmonary translocation of intratracheal-instilled particles in vivo in rats: Effect of lipopolysaccharide. *Toxicology* **222,** 195–201.

Chen, X., and Schluesener, H. J. (2008). Nanosilver: A nanoproduct in medical application. *Toxicol. Lett.* **176,** 1–12.

Davis, J. M., and Svendsgaard, D. J. (1990). U-shaped dose-response curves: Their occurrence and implications for risk assessment. *J. Toxicol. Environ. Health* **30,** 71–83.

Elder, A., Gelein, R., Silva, V., Feikert, T., Opanashuk, L., Carter, J., Potter, R., Maynard, A., Ito, Y., Finkelstein, J., *et al.* (2006). Translocation of inhaled ultrafine manganese oxide particles to the central nervous system. *Environ. Health Perspect.* **114,** 1172–1178.

Graf, P., Mantion, A., Foelske, A., Shkilnyy, A., Masic, A., Thünemann, A. F., and Taubert, A. (2009). Peptide-coated silver nanoparticles: Synthesis, surface chemistry, and pH-triggered, reversible assembly into particle assemblies. *Chem. Eur. J.* **15,** 5831–5844.

Gramowski, A., Flossdorf, J., Bhattacharya, K., Jonas, L., Lantow, M., Rahman, Q., Schiffmann, D., Weiss, D. G., and Dopp, E. (2010). Nanoparticles induce changes of the electrical activity of neuronal networks on microelectrode array neurochips. *Environ. Health Perspect.* **118,** 1363–1369.

Guerrero, S., Araya, E., Fiedler, J. L., Arias, J. I., Adura, C., Albericio, F., Giralt, E., Arias, J. L., Fernández, M. S., and Kogan, M. J. (2010). Improving the brain delivery of gold nanoparticles by conjugation with an amphipathic peptide. *Nanomedicine* **5,** 897–913.

Haase, A., Arlinghaus, H. F., Tentschert, J., Jungnickel, H., Graf, P., Mantion, A., Draude, F., Galla, S., Plendl, J., Goetz, M. E., *et al.* (2011). Application of laser postionization secondary neutral mass spectrometry/time-of-flight secondary ion mass spectrometry in nanotoxicology: Visualization of nanosilver in human macrophages and cellular responses. *ACS Nano.* **5,** 3059–3068.

Hussain, S. M., Javorina, A. K., Schrand, A. M., Duhart, H. M., Ali, S. F., and Schlager, J. J. (2006). The interaction of manganese nanoparticles with PC-12 cells induces dopamine depletion. *Toxicol. Sci.* **92,** 456–463.

Ji, J. H., Jung, J. H., Kim, S. S., Yoon, J. U., Park, J. D., Choi, B. S., Chung, Y. H., Kwon, I. H., Jeong, J., Han, B. S., *et al.* (2007). Twenty-eight-day inhalation toxicity study of silver nanoparticles in Sprague-Dawley rats. *Inhal. Toxicol.* **19,** 857–871.

Johnson, P. B., and Christy, R. W. (1972). Optical constants of the noble metals. *Phys. Rev. B* **6,** 4370–4379.

Kahlert, S., Zündorf, G., and Reiser, G. (2005). Glutamate-mediated influx of extracellular Ca^{2+} is coupled with reactive oxygen species generation in cultures hippocampal neurons but not in astrocytes. *J. Neurosci. Res.* **79,** 262–271.

Kreyling, W. G., Semmler-Behnke, M., and Möller, W. (2006). Health implications of nanoparticles. *J. Nanopart. Res.* **8,** 543–562.

Kreyling, W., Semmler-Behnke, M., Seitz, J., Scymczak, W., Wenk, A., Mayer, P., Takenaka, S., and Oberdörster, G. (2009). Size dependence of the translocation of inhaled iridium and carbon nanoparticle aggregates from the lung of rats to the blood and secondary target organs. *Inhal. Toxicol.* **21,** 55–60.

Liu, Z., Ren, G., Zhang, T., and Yang, Z. (2009). Action potential changes associated with the inhibitory effects on voltage-gated sodium currents of hippocampal CA1 neurons by silver nanoparticles. *Toxicology* **264,** 179–184.

Liu, Z., Ren, G., Zhang, T., and Yang, Z. (2011). The inhibitory effects of nano-Ag on voltage-gated potassium currents of hippocampal CA1 neurons. *Environ. Toxicol.* **26,** 552–558.

Downloaded from http://toxsci.oxfordjournals.org/ at Bundesinstitut fuer Gesundheitlich on July 24, 2014

Manev, H., Caredda, S., and Gravson, D. R. (1991). Nonselective inhibition by antisense oligonucleotides of cytosine arabinoside action. *Neuroreport* **2,** 589–592.

Maragakis, N. J., and Rothstein, J. D. (2006). Mechanisms of disease: Astrocytes in neurodegenerative disease. *Nat. Clin. Pract. Neurol.* **2,** 679–689.

Mates, J. M., Perez-Gomez, G., and Nunez de Castro, I. (1999). Antioxidant enzymes and human diseases. *Clin. Biochem.* **32,** 595–603.

Oberdörster, E. (2004). Manufactured nanomaterials (fullerenes, C60) induce oxidative stress in the brain of juvenile largemouth bass. *Environ. Health Perspect.* **112,** 1058–1062.

Oberdörster, G., Elder, A., and Rinderknecht, A. (2009). Nanoparticles and the brain: Cause of concern? *J. Nanosci. Nanotechnol.* **9,** 4996–5007.

Oberdörster, G., Oberdörster, E., and Oberdörster, J. (2005). Nanotoxicology: An emerging discipline evolving from studies of ultrafine particles. *Environ. Health Perspect.* **113,** 823–839.

Oberdörster, G., Sharp, Z., Atudorei, V., Elder, A., Gelein, R., Kreyling, W., and Cox, C. (2004). Translocation of inhaled ultrafine particles to the brain. *Inhal. Toxicol.* **16,** 437–445.

Rahman, M. F., Wang, J., Patterson, T. A., Saini, U. T., Robinson, B. L., Newport, G. D., Murdock, R. C., Schlager, J. J., Hussain, S. M., and Ali, S. F. (2009). Expression of genes related to oxidative stress in the mouse brain after exposure to silver-25 nanoparticles. *Toxicol. Lett.* **187,** 15–21.

Richardson, K. C., Jarett, L., and Finke, E. H. (1960). Embedding in epoxy resins for ultrathin sectioning in electron microscopy. *Stain. Technol.* **35,** 313–323.

Robinette, B. L., Harrill, J. A., Mundy, W. R., and Shafer, T. J. (2011). In vitro assessment of developmental neurotoxicity: Use of microelectrode arrays to measure functional changes in neuronal network ontogeny. *Front. Neuroeng.* **4,** 1–9.

Rousseau, V., Denizot, B., Pouliquen, D., Jallet, P., and Le Jeune, J. J. (1997). Investigation of blood-brain barrier permeability to magnetite-dextran nanoparticles (MD3) after osmotic disruption in rats. *MAGMA* **5,** 213–222.

Rungby, J., and Danscher, G. (1983). Localization of exogenous silver in brain and spinal cord of silver exposed rats. *Acta Neuropathol.* **60,** 92–98.

Sharma, H. S., and Sharma, A. (2007). Nanoparticles aggravate heat stress induced cognitive deficits, blood-brain barrier disruption, edema formation and brain pathology. *Prog. Brain Res.* **162,** 245–273.

Smith, M. P., and Wayne, A. (2007). Oxidative stress and dopamine depletion in an intrastriatal 6-hydroxydopamine model of Parkinson's disease. *Neuroscience* **144,** 1057–1066.

Sompol, P., Ittarat, W., Tangpong, J., Chen, Y., Doubinskala, I., Batinic-Haberle, I., Abdul, H. M., Butterfield, D. A., and St Clair, D. K. (2008). A neuronal model of Alzheimer's disease: An insight into the mechanisms of oxidative stress-mediated mitochondrial injury. *Neuroscience* **153,** 120–130.

Tang, J., Xiong, L., Wang, S., Wang, J., Liu, L., Li, J., Yuan, F., and Xi, T. (2009). Distribution, translocation and accumulation of silver nanoparticles in rats. *J. Nanosci. Nanotechnol.* **9,** 4924–4932.

Tang, J., Xiong, L., Zhou, G., Wang, S., Wang, J., Liu, L., Li, J., Yuan, F., Lu, S., Wan, Z., *et al.* (2010). Silver nanoparticles crossing through and distribution in the blood-brain barrier in vitro. *J. Nanosci. Nanotechnol.* **10,** 6313–6317.

Trickler, W. J., Lantz, S. M., Murdock, R. C., Schrand, A. M., Robinson, B. L., Newport, G. D., Schlager, J. J., Oldenburg, S. J., Paule, M. G., Slikker, W., Jr, *et al.* (2010). Silver nanoparticle induced blood-brain barrier inflammation and increased permeability in primary rat brain microvessel endothelial cells. *Toxicol. Sci.* **118,** 160–170.

Wang, J., Rahman, M. F., Duhart, H. M., Newport, G. D., Patterson, T. A., Murdock, R. C., Hussain, S. M., Schlager, J. J., and Ali, S. F. (2009). Expression changes of dopaminergic system-related genes in PC12 cells induced by manganese, silver, or copper nanoparticles. *Neurotoxicology* **30,** 926–933.

Wang, Y., Luo, W., and Reiser, G. (2007). Activation of protease-activated receptors in astrocytes evokes a novel neuroprotective pathway through release of chemokines of the growth-regulated oncogene/cytokine-induced neutrophil chemoattractant family. *Eur. J. Neurosci.* **26,** 3159–3168.

Zhaowei, L., Guogang, R., Tao, Z., and Zhuo, Y. (2009). Action potential changes associated with the inhibitory effects on voltage-gated sodium current of hippocampal CA1 neurons by silver nanoparticles. *Toxicology* **264,** 179–184.

Downloaded from http://toxsci.oxfordjournals.org/ at Bundesinstitut fuer Gesundheitlich on July 24, 2014